HHS Public Access

Author manuscript

MAGMA. Author manuscript; available in PMC 2016 April 01.

Published in final edited form as:

MAGMA. 2015 April ; 28(2): 195–205. doi:10.1007/s10334-014-0455-2.

Development and performance of a 129-GHz dynamic nuclear polarizer in an ultra-wide bore superconducting magnet

Lloyd L. Lumata,
Advanced Imaging Research Center, University of Texas Southwestern Medical Center, 5323 Harry Hines Boulevard, Dallas, TX 75390, USA

Richard Martin,
Advanced Imaging Research Center, University of Texas Southwestern Medical Center, 5323 Harry Hines Boulevard, Dallas, TX 75390, USA

Ashish K. Jindal,
Advanced Imaging Research Center, University of Texas Southwestern Medical Center, 5323 Harry Hines Boulevard, Dallas, TX 75390, USA

Zoltan Kovacs,
Advanced Imaging Research Center, University of Texas Southwestern Medical Center, 5323 Harry Hines Boulevard, Dallas, TX 75390, USA

Mark S. Conradi, and
Department of Physics, Washington University, St. Louis, MO 63130, USA

Matthew E. Merritt
Advanced Imaging Research Center, University of Texas Southwestern Medical Center, 5323 Harry Hines Boulevard, Dallas, TX 75390, USA. Departments of Biomedical Engineering and Molecular Biophysics, University of Texas Southwestern Medical Center, 5323 Harry Hines Boulevard, Dallas, TX 75390, USA. Department of Bioengineering, University of Texas at Dallas, 800 West Campbell Road, Richardson, TX 75080, USA

Matthew E. Merritt: matthew.merritt@utsouthwestern.edu

Abstract

Objective—We sought to build a dynamic nuclear polarization system for operation at 4.6 T (129 GHz) and evaluate its efficiency in terms of ^{13}C polarization levels using free radicals that span a range of ESR linewidths.

Materials and methods—A liquid helium cryostat was placed in a 4.6 T superconducting magnet with a 150-mm warm bore diameter. A 129-GHz microwave source was used to irradiate ^{13}C enriched samples. Temperatures close to 1 K were achieved using a vacuum pump with a 453-m^3/h roots blower. A hyperpolarized ^{13}C nuclear magnetic resonance (NMR) signal

Correspondence to: Matthew E. Merritt, matthew.merritt@utsouthwestern.edu.

Conflict of interest None.

Ethical standard The manuscript does not contain animal studies or clinical studies/patient data.

was detected using a saddle coil and a Varian VNMRS console operating at 49.208 MHz. Samples doped with free radicals BDPA (1,3-bisdipheny-lene-2-phenylallyl), trityl OX063 (tris{8-carboxyl-2,2,6,6-benzo(1,2-d:4,5-d)-bis(1,3)dithiole-4-yl}methyl sodium salt), galvinoxyl ((2,6-di-tert-butyl-α-(3,5-di-tert-butyl-4-oxo-2,5-cyclohexadien-1-ylidene)-*p*-tolyloxy), 2,2-diphenylpicrylhydrazyl (DPPH) and 4-oxo-TEMPO (4-Oxo-2,2,6,6-tetramethyl-1-piperidinyloxy) were assayed. Microwave dynamic nuclear polarization (DNP) spectra and solid-state ^{13}C polarization levels for these samples were determined.

Results—^{13}C polarization levels close to 50 % were achieved for [1-^{13}C]pyruvic acid at 1.15 K using the narrow electron spin resonance (ESR) linewidth free radicals trityl OX063 and BDPA, while 10–20 % ^{13}C polarizations were achieved using galvinoxyl, DPPH and 4-oxo-TEMPO.

Conclusion—At this field strength free radicals with smaller ESR linewidths are still superior for DNP of ^{13}C as opposed to those with linewidths that exceed that of the ^{1}H Larmor frequency.

Keywords

Nuclear magnetic resonance; Electron spin resonance; Free radicals; Hyperpolarization

Introduction

Due to its specificity, nuclear magnetic resonance (NMR) has been a standard analytical tool for molecular structure elucidation in chemistry, materials science, biology and medicine. However, despite its usefulness in these areas, NMR spectroscopy (MRS) and imaging (MRI) especially of low-gamma (γ) nuclei such as ^{13}C (γ = 10.7 MHz/T) can be challenging due to low signal sensitivity and prohibitively long measurement times. As dictated by Boltzmann statistics, the relatively weak magnetic moments of nuclear spins lead to minute differences in the nuclear spin populations between the Zeeman energy levels at ambient conditions. Thus, the polarization level *P*, which is equal to the surplus number of nuclear spins residing in a particular Zeeman energy level, is on the order of ppm at achievable field strengths [1].

On the other hand, electron spins (γ_e = 28,000 MHz/T) have a relatively high degree of polarization due to their large magnetic moments. In fact, at moderate magnetic fields (e.g., W-band field or 3.35 T) and temperatures close to 1 K, electron polarization is over 90 %, whereas ^{13}C spin polarization is still miniscule, with *P* significantly less than 1 %. Overhauser predicted in 1953 that polarization transfer from electrons to nuclei could be achieved by irradiation at the electron Larmor frequency [2], and experimental proof of this phenomenon was realized a few years later in the Slichter lab [3]. Later on a more general off-resonance microwave irradiation technique, known as dynamic nuclear polarization (DNP), was used to amplify the NMR signals of dielectric solids at low temperature and in a high magnetic field. Since the 1960s the DNP technique has been used largely in the production of polarized targets for neutron scattering and hadron physics research under cryogenic conditions [4, 5]. In addition, thanks to the vision of a select group of spectroscopists, it has found application in NMR structure determination in the solid state [6]. It was not until 2003 with the invention of the dissolution method that the power of NMR signal amplification by DNP became accessible at physiologically tolerable

temperatures for biomedical MRS and MRI research [7]. In this method the frozen polarized sample is rapidly dissolved with pressurized hot water or other solvents thereby producing an injectable MR-based molecular imaging agent [7]. Consequently, the liquid-state NMR signals of biomolecules are dramatically enhanced for biomedical magnetic resonance [8, 9]. In this case the liquid state hyperpolarized NMR signal decays due to the T_1 of the spins and the applied excitation pulses. Efficiency of the DNP process depends upon many factors including the microwave irradiation power, temperature of the sample and magnetic field strength; these parameters are relatively easy to control in an experimental setting [10, 11]. Other factors include ESR properties of the free radicals, glassing conditions and the relaxation leakage factor of the target nuclear spins [4, 12–14].

To ensure that high signal enhancements are achieved in the liquid state it is of paramount importance that the frozen samples have optimal solid-state nuclear polarization prior to dissolution. Several designs of DNP instrumentation have been described before to achieve the desired enhanced nuclear polarization. The pioneering instrumentation work of Ardenkjaer-Larsen et al. [7] used an in situ cryostat that draws in liquid Helium from the main liquid helium (LHe) reservoir of a 3.35 T superconducting magnet. Another dissolution DNP design was described by Comment et al. using a continuous flow cryostat in which LHe is drawn from a nearby storage cryostat [15, 16]. Similar continuous-flow DNP cryostats have been reported with multiple sample capability [17, 18]. The use of a super-wide bore magnet with a continuous-flow cryostat for dissolution DNP has been previously reported by Cremillieux et al. [18]. Commercial dissolution DNP polarizers are also available, such as the HyperSense (Oxford Instruments, England); recently, a DNP hyperpolarizer intended for sterile use was reported [19]. Herein we present the construction of a homebuilt DNP polarizer that is based on a design tailored to an ultra-wide bore (150 mm) superconducting magnet and a non-continuous flow, large LHe volume hold cryostat. The relatively large LHe reserve capacity (9 L) of our DNP cryostat allows long, autonomous operation of the polarizer for up to 10–12 h. Unlike the commercial DNP polarizer or its prototypes, our DNP cryostat is separated from the superconducting magnet, allowing ease of use and maintenance. In addition, our DNP probe is detachable from the cryostat which allows easy access for maintenance, repairs or modification. The base operating temperature of our DNP polarizer with pumping from the roots blower was 1.15 K. Performance of the polarizer was evaluated by DNP of ^{13}C-enriched substrates using different free radical polarizing agents commonly used for dissolution DNP: BDPA, trityl OX063, galvinoxyl, DPPH and 4-oxo-TEMPO [7, 13, 15, 20–22]. The main goal of this research therefore was to construct a dynamic nuclear polarizer based on the advantages offered by an ultra-wide bore superconducting magnet and evaluate its efficiency in terms of ^{13}C polarization levels using a range of free radical polarizing agents.

Materials and methods

General DNP design

The schematic diagram of the homebuilt DNP polarizer (Fig. 1) is similar in overall design aspects to the dissolution DNP polarizers previously reported in literature [7, 15–19]. The common theme for all DNP instrumentation is that it should be able to: (1) subject the target

sample (typically up to several hundred microliters in volume) to temperatures close to 1 K; (2) subject the target sample to a strong magnetic field so that the electron spin polarization is close to unity; and, (3) transfer the high electron polarization to the nuclear spins via off-resonance microwave irradiation under those conditions. The main parts of a DNP polarizer are therefore: (1) an external magnetic field source typically provided by a superconducting magnet; (2) a cryostat; (3) a microwave system; (4) a DNP probe insert for the dissolution process; (5) a vacuum system; and, (6) an NMR circuit for observing the magnetization. Finally, a dissolution system is needed to produce the hyperpolarized MR imaging solution.

Magnet system

The high external magnetic field required to achieve electron spin polarization close to unity at cryogenic temperatures was provided by an ultra-wide bore (150 mm) Bruker superconducting magnet (Bruker Corporation, Billerica, MA). During the installation this unshielded Bruker magnet was ramped up to a field of 4.6 T, which corresponds to a proton Larmor frequency of 195.68 MHz, or an ESR frequency of 129 GHz.

Cryostat

Our custom-built cryostat (Kadel Engineering Corp., Danville, IN) shown in Fig. 2 is based on a previously published design of a cryogenic research dewar [23] which has its own LHe (9 L capacity) and liquid nitrogen (LN_2, 5 L capacity) reservoirs. An aluminum thermally conducting shield is connected to the LN_2 vessel surrounding the upper region of the LHe vessel. A vacuum wall with several layers of Mylar sheets surrounds the LN_2 and LHe reservoirs. The cryostat sits atop the superconducting magnet with its tail (14.73 cm OD, 5.71 cm ID, 113 cm length) extending down to the field center of the magnet's room temperature bore. The cryostat body (22.35 cm OD, 40.64 cm length) fits between the stacks of the magnet. A 7.11-cm long neck extends on top of the cryostat that also contains a KF50 pumping port on the side. LHe flow from the main reservoir to the sample space (5.71 cm diameter) is controlled by a stainless steel needle valve. The top part of the cryostat is shown in Fig. 2b, which displays the LHe and LN_2 filling ports as well as the needle valve knob.

DNP probe insert

The DNP probe insert is a removable assembly consisting of the liquid helium level sensor, temperature sensor, microwave waveguide and cavity, NMR circuit and the elevator. As displayed in Fig. 3, the DNP probe insert consists of two main tubes: a fixed Garolite tube that holds the NMR saddle coil and microwave cavity at the bottom, and a sliding inner G-10 fiberglass tube that contains the sample cup. The outer tube also provides structural integrity for the other probe pieces such as the microwave waveguide, liquid helium level sensor (American Magnetics Inc, Oak Ridge, TN), temperature sensor (LakeShore Cryotronics, Westerville, OH) and the NMR coaxial lines. These probe components are secured by copper disks that also act as heat shields. The bottom part of the sliding inner tube was perforated for easy cryogen access to the sample. During the dissolution process the inner tube is lifted about 12–16 cm from its normal operating position (sample cup is at the center of the microwave cavity) to avoid contact with the liquid helium bath. A removable 1.905-cm brass plug with silicon O-ring (Swagelok Inc., Solon, OH) is used to seal the top of the sliding inner tube.

NMR system

A remote-tuning NMR circuit design was used for NMR detection since the NMR coil is immersed in LHe [24]. A 0.216-cm OD 50-Ohm copper coaxial line (RF Connections Inc., Gaithersburg, MD) was used as the NMR transmission line inside the cryostat. A rectangular saddle coil with a 1-inch ID was wrapped around the bottom of the fixed outer tube using Teflon tape, intending to cover the DNP sample cup volume. The rectangular saddle coil was positioned in such a way that microwaves pass through its center without deterrence. Tuning was done outside the cryostat by a series-tuned, parallel-matched NMR circuit box using variable glass capacitors (Voltronics Inc., Salisbury, MD). The ^{13}C NMR probe was tuned and matched at 49.208 MHz. A Varian VNMRS 400 spectrometer (Agilent Technologies, Santa Clara, CA) was used for NMR detection.

Microwave system

The schematic diagram for the 129-GHz microwave system used for DNP is shown in Fig. 4a. Our microwave source (Virginia Diodes Inc., Charlottesville, VA) is a phase-locked dielectric resonant oscillator (PDRO) with a maximum power output of 120 mW. For power attenuation and detection the rectangular waveguide source output WR-08 can be connected to a variable attenuator then to a 3-port circulator where a tiny portion of the microwave power is diverted to a diode detector (Millitech Inc., Northampton, MA). As shown in the Fig. 4a schematics, the power attenuation-detection system can be bypassed by connecting the WR-08 rectangular source output directly to a 90° E-plane bend and then to a rectangular-to-circular transition CR-08 (Millitech Inc., Northampton, MA). A homebuilt adapter is connected between the CR-08 circular output and a thin-walled, quarter-inch OD stainless tube (Oxford Instruments, Concord, MA) that serves as an oversized cylindrical waveguide. A 0.381-mm thick Teflon PTFE sheet (Small Parts Inc., Miami Lakes, FL) was clamped between the homebuilt circular adapter and the rectangular-to-circular transition piece acted as a vacuum seal. A 2.86-cm OD, 3.81-cm long bottom-sealed copper pipe was used as the microwave cavity. Microwave frequency sweep control was done using a PTS 160 frequency synthesizer (Programmed Test Sources Inc., Littleton, MA) where the resulting microwave frequency is given by $f(\text{GHz}) = 12.9 * f_{\text{PTS}}(\text{MHz})$. The microwave sweep is accessible in the range 128.5–129.5 GHz with a sweep step resolution of less than 1 MHz.

Liquid helium level, temperature and pressure sensors

Liquid helium level sensors (American Magnetics Inc., Oak Ridge, TN) were installed in the main reservoir of the cryostat as well as in the sample space (mounted on the DNP probe insert). The sensors are made of fine superconducting filament contained within a 0.635-cm OD G-10 tube. The liquid level measurements were made by measuring the resistance of the filament using a Model 135-2 K level monitor (American Magnetics Inc., Oak Ridge, TN). For vacuum pressure readout, a MEMS Pirani transducer (Kurt J. Lesker Co., Jefferson Hills, PA) with a 10^{-5} torr-1 atm readout range was mounted on the cryostat; this transducer is protected by a KF16 butterfly valve that is closed during the dissolution process when the cryostat is pressurized with Helium gas. In addition, an analog Bourdon dial pressure gauge (Kurt J. Lesker Co., Jefferson Hills, PA) was also installed on the cryostat to provide a crude

but fast readout of the cryostat sample space pressure. Sample temperature can be estimated from the LHe vapor pressure. For complimentary temperature measurement a Cernox CX-1070-AA sensor (Lake Shore Cryotronics, Westerville, OH) was mounted near the bottom of the microwave cavity. Temperature was estimated from the four-wire resistance measurement of the Cernox sensor using a Keithley 2000 digital multimeter (Keithley Instruments Inc., Cleveland, OH).

Vacuum pump and gas supply

A 4-way KF-50 cross vacuum fitting (Kurt J. Lesker Co., Jefferson Hills, PA) was clamped on the top hat side of the cryostat for gas pumping and pressurizing of the sample space. A 1.5-m stainless steel KF50 flexible hose connects the cryostat to an Oerlikon-Leybold WSU501/D65B vacuum pump with a 453-m^3/h roots blower (Oerlikon-Leybold Vacuum, Export, PA) to achieve a temperature close to 1 K in the sample space. The aforementioned digital and analog pressure sensors were installed on one side of the 4-way cross, while the remaining port serves as a valve-controlled inlet for high pressure helium gas.

Free radicals, ^{13}C substrates and glassing solvents

The free radical trityl OX063 (tris{8-carboxyl-2,2,6,6-benzo(1,2-d:4,5-d)-bis(1,3)dithiole-4-yl}methyl sodium salt) was purchased from Oxford Instruments Molecular Biotools (Tubney Woods, UK). The free radicals BDPA, galvinoxyl, DPPH and 4-oxo-TEMPO were obtained from Sigma Aldrich (St. Louis, MO). The ^{13}C-enriched substrates [1-^{13}C]pyruvic acid, [1-^{13}C]sodium pyruvate and [1-^{13}C]ethyl acetate as well as the glassing solvents (sulfolane, dimethyl sulfoxide, glycerol, water) were obtained from commercial sources (Sigma-Aldrich, St. Louis, MO and Cambridge Isotope Laboratories, Andover, MA) and were used without further purification.

Preparation of DNP samples

(1) Trityl OX063: 4.28 mg trityl OX063 was dissolved in 200 μL neat [1-^{13}C]pyruvic acid. The final concentration of trityl OX063 in the solution was 15 mM. (2) BDPA: 4 mg BDPA was dissolved in 100 μL sulfolane via sonication as described previously [20]. The solution was then mixed with 100 μL neat [1-^{13}C]pyruvic acid. The final concentration of BDPA in the mixture was 20 mM. (3) Galvinoxyl: 3.37 mg galvinoxyl was dissolved in 100 μL [1-^{13}C]ethyl acetate then mixed with an equal volume of DMSO. The final concentration of galvinoxyl in the solution was 40 mM [21]. (4) DPPH: 1.58 mg of DPPH was dissolved in 100 μL sulfolane then mixed with 100 μL [1-^{13}C]ethyl acetate. The final concentration of DPPH in the solution was 20 mM [22]. (5) 4-Oxo-TEMPO: 31.1 mg [1-^{13}C]sodium pyruvate was dissolved in a 200 μL solution containing 1:1 v/v glycerol:water. 1.36 mg 4-oxo-TEMPO was mixed into the solution where the final concentration of the free radical was 40 mM. Overall, a total of 15 DNP samples (3 aliquots for each free radical) were prepared and measured.

^{13}C microwave frequency sweeps

The ^{13}C DNP spectrum, a plot of the ^{13}C NMR intensity or polarization as a function of microwave irradiation frequency near the free radical ESR resonant frequency, was recorded

by applying a 10° rf pulse after 3-min of microwave irradiation at each microwave frequency. Prior to recording the NMR intensity at the next microwave sweep frequency a series of hard RF pulses was applied to destroy the remnant ^{13}C polarization from the previous frequency point. The two optimum microwave irradiation frequencies for ^{13}C DNP, the positive P(+) and negative P(−) polarization peaks, were identified for each free radical polarizing agent.

Measurement of ^{13}C polarization

200 μL aliquots of DNP samples doped with different free radicals (see Table 1) were polarized at their corresponding P(+) optimum microwave frequencies at 4.6 T and 1.15 K. Growth of the ^{13}C polarization under microwave irradiation was monitored by applying a 2° flip-angle pulse every 2 or 5 min. Polarization buildup curves were fitted with a single exponential buildup equation $P(t) = P_0[1 - \exp(-t/\tau_{bu})]$ where P_0 is the maximum ^{13}C NMR intensity/polarization, t is the microwave irradiation time and τ_{bu} is the polarization buildup time constant. The DNP-enhanced polarization P_{dnp} was calculated by multiplying the experimentally-determined NMR signal enhancement ε (ratio of the integrated NMR signals in the hyperpolarized state over the thermal equilibrium state) and the calculated ^{13}C (γ_n = 10.705 MHz/T) thermal polarization P_{th} at 4.6 T and 1.15 K, where in this case, $P_{th} = \tanh(\mu B/kT)$ = 0.103 %. NMR spectra were processed using an ACD 1D NMR processor, version 12 (Advanced Chemistry Development, Toronto, Canada). Data analyses were done using Igor Pro version 6 (Wavemetrics Inc., Portland, OR).

Results

Magnet system

The large bore size (150 mm) of the magnet allowed us to design a cryostat with a sample space large enough for a large sample cup (600 μL maximum cup volume), an elevator to remove the sample from the LHe prior to dissolution, LHe level and temperature sensors, a microwave waveguide that irradiates the sample cavity from the side, and an NMR circuit. The large bore of the superconducting magnet allows a relatively large volume hold (9 L) of the cryostat.

Cryostat and vacuum system

LHe flow into the sample space is manually set by a needle valve with a control knob atop the cryostat. Figure 2c shows that the vapor pressure in the sample space can go down to 0.43 Torr with the 453-m^3/h roots blower pump on. This LHe vapor pressure corresponds to a base temperature of 1.15 K for a sample immersed in about 10 cm of LHe [25]. Figure 2d shows the LHe consumption rate for a full 9-L cryostat when the vacuum pump is on (0.75 L/h at 0.43 Torr) or off (0.36 L/h at ~760 Torr). When both the microwave source and pump are turned on the LHe consumption rate is about 0.8 L/h. The cryostat, when filled to its full capacity, could consistently sustain 10 h of continuous DNP operation (target sample cooled to 1.15 K under microwave irradiation) without LHe refilling.

Microwave system

The experimental threshold microwave power needed to achieve maximum ^{13}C signal enhancement was about 20 mW, as shown in Fig. 4b. The variable attenuator-circulator-diode detector components of the microwave system can be bypassed without diminishing DNP efficiency. In this case we removed the attenuator-circulator-diode detector system for the consequent ^{13}C polarization experiments and, as such, the power output right after the microwave source is 120 mW. Our oversized waveguide is approximately a meter-long and we currently have no information on the microwave power output at the waveguide's terminal. Nevertheless, the power range output 20–120 mW yields the maximum ^{13}C DNP signal using our homebuilt DNP system. The 129-GHz microwave source has a large sweepable frequency range (1,000 MHz) that can encompass the ^{13}C microwave DNP spectra of samples doped with large ESR linewidth free radicals such as 4-oxo-TEMPO.

^{13}C microwave DNP spectra

Prior to measuring the actual ^{13}C polarization values we first determined the optimum microwave irradiation frequencies $P(+)$ and $P(-)$ for ^{13}C DNP (see Table 1). The ^{13}C microwave DNP spectra, which show the ^{13}C NMR signal enhancements as a function of microwave frequency sweep near the ESR frequency ν_e of the free radical, are displayed in Fig. 5. The normalized ^{13}C microwave DNP spectra in Fig. 5 were arranged according to increasing ESR linewidths of the free radicals used [13]. Separation between ^{13}C $P(+)$ and $P(-)$ for each free radical are as follows: BDPA (40 MHz), trityl OX063 (60 MHz), galvinoxyl (130 MHz), DPPH (130 MHz) and 4-oxo-TEMPO (460 MHz).

^{13}C polarization levels

For consistency, the DNP-enhanced ^{13}C polarization measurements reported here were taken by irradiating the samples at their corresponding $P(+)$ microwave frequencies. Figure 6a shows representative ^{13}C NMR spectra in the hyperpolarized state and at thermal equilibrium at 4.6 T and 1.15 K for a neat [1-^{13}C]pyruvic acid sample doped with 15 mM trityl OX063. The ratio of the integrated NMR areas of the hyperpolarized NMR signal over the thermal NMR signal was 530, which corresponds to 54 % ^{13}C polarization at 4.6 T and 1.15 K. As displayed in Table 1 and Fig. 6, the average ^{13}C polarization ($N = 3$) for ^{13}C samples doped with different free radicals achieved are: BDPA (46.5 ± 3.9 %), trityl OX063 (54.4 ± 4.2 %), galvinoxyl (10.5 ± 1.7 %), DPPH (13.3 ± 2.4 %) and 4-oxo-TEMPO (18.3 ± 3.8 %).

Discussion

Instrumentation

The dissolution DNP polarizer [7] and the commercial HyperSense polarizer (Oxford Instruments, UK) operate at 3.35 T, which requires a microwave source frequency close to 95 GHz (W-band). We opted to use a higher magnetic field (4.6 T) since preliminary reports have shown that a higher field yields higher nuclear polarization in DNP [10, 11, 16, 26]. The prototype 3.35 T dissolution DNP polarizer [7] and the HyperSense commercial polarizer have a cryostat/variable temperature insert (VTI) that draws LHe from the main

reservoir of the superconducting magnet. Unlike these systems, our cryostat is not permanently tied to the polarizer, thus allowing easy access for repairs or thawing in case there is an ice block in the needle valve system. In other homebuilt DNP systems cryostats built for 89 mm-bore superconducting magnets require removal of the microwave waveguide prior to dissolution [15, 16]. In our case, the waveguide is permanently mounted to the side of the microwave cavity. Moreover, the large sample space allows use of a relatively bigger sample cup (600 μL capacity) in case there is need for high concentration/high volume dissolution liquids. Other groups have reported homebuilt polarizers with multi-sample capability [17, 18]. All these polarizers have continuous-flow cryostats where a transfer line is connected to a LHe dewar during DNP operation. Alternatively, the new clinical DNP polarizer dubbed SpinLAB (GE Healthcare, Menlo Park, CA) has a multi-sample capability, a LHe recovery system and sterile sample processing [19]. However, the cost of the clinical use polarizer is beyond the means of most basic science departments. The total cost of our homebuilt DNP polarizer, minus the cost of superconducting magnet, is less than USD 100,000, a small fraction of the cost of commercial preclinical and clinical DNP polarizers.

Sample compatibility

^{13}C DNP samples were doped with optimum concentrations of different free radical polarizing agents commonly used for dissolution DNP: BDPA (20 mM), trityl OX063 (15 mM), galvinoxyl (40 mM), DPPH (20 mM) and 4-oxo-TEMPO (40 mM) [7, 15, 20–22]. We note that of these free radicals only trityl OX063 and 4-oxo-TEMPO are water-soluble whereas BDPA, galvinoxyl and DPPH are soluble in less polar solvents such as sulfolane or ethyl acetate [20–22]. Trityl OX063 and BDPA were used to polarize [1-^{13}C]pyruvic acid samples, 4-oxo-TEMPO for [1-^{13}C]sodium pyruvate, while DPPH and galvinoxyl were used for DNP of [1-^{13}C]ethyl acetate. The choice of these ^{13}C samples is mainly due to compatibility; the latter three free radicals 4-oxo-TEMPO, galvinoxyl and DPPH apparently react with pyruvic acid and produce negligible DNP enhancements [21, 22, 27]. On the other hand, ethyl acetate is a good solvent for both galvinoxyl and DPPH, thus its ^{13}C-enriched equivalent is an excellent choice to test for DNP using these two free radicals.

^{13}C microwave DNP spectra

A characteristic feature of the microwave DNP spectrum is the presence of two maxima in the ^{13}C NMR intensity vs microwave frequency plot: the positive polarization peak $P(+)$, designated by an up arrow in Fig. 5, corresponds to positive spin temperature T_s and the negative polarization peak $P(-)$, denoted by the down arrow, corresponds to negative T_s. In the solid effect regime where the ESR linewidth D is much smaller than the nuclear Larmor frequency ν_n these optimum polarization peaks are expected to appear at $\nu_e \pm \nu_n$ [4, 5]. However, considering the ESR linewidths of these free radicals are wider than or comparable to the ^{13}C ν_n, the expected predominant DNP mechanism for ^{13}C samples here is the thermal mixing process [28, 29]. The shape of the microwave DNP spectra in this regime can be approximated by the Borghini model, which predicts the nuclear spin temperature as a function of the ESR line shape [30]. The actual microwave DNP spectra have some deviations from the Borghini model, which can be explained by considering the partial microwave saturation effect in the DNP setup [31]. In a previous W-band ESR study

it was determined that the ESR *D* of these free radicals at (2 % height from the base) are: BDPA (63 MHz), trityl OX063 (115 MHz), galvinoxyl (250 MHz), DPPH (290 MHz) and 4-oxo-TEMPO (465 MHz) [13]. The microwave DNP spectra of ^{13}C samples doped with different free radicals in Fig. 5 are arranged according to increasing ESR linewidths. Inspection of Fig. 5 reveals that the polarization peak separation $|P(+)\text{-}P(-)|$ scales with the ESR *D* of the free radical polarizing agent, indicating agreement with the Borghini model [30].

^{13}C polarization levels—The ^{13}C polarization buildup curves of ^{13}C-enriched samples doped with different free radicals are shown in Fig. 6b. The buildup curves can be fitted with a single-exponential equation with a time constant τ_{bu}. There is great variability in the buildup time constants depending upon sample composition. In general, polarization buildup kinetics are mainly dependent upon: (1) density of electron spin pumping centers as determined by the optimum free radical concentration; and, (2) density of nuclear spins where shorter inter-nuclear spin distances favors faster DNP buildup via the nuclear spin diffusion process [32].

Figure 6c displays the temperature dependence of electron and ^{13}C spin Boltzmann thermal polarization levels at 4.6 T vis-à-vis the ^{13}C polarization levels achieved with different free radicals. Under the operating conditions of the polarizer the electron spin thermal polarization is almost unity (99.1 %) whereas the ^{13}C nuclear spin thermal polarization is still low (0.103 %). On the experimental side it is evident that the enhancement values of ^{13}C NMR signals via DNP depend largely on the type of free radical polarizing agents used. The highest ^{13}C polarization values were achieved using the narrow-ESR *D* free radicals BDPA and trityl OX063 with ^{13}C polarization values close to 50 %. On the other hand, the relatively wider ESR *D* free radicals galvinoxyl, DPPH and 4-oxo-TEMPO yielded polarization levels in the range 10–20 %. Variability in the ^{13}C polarization levels may be ascribed to the effect of the free radical ESR properties on DNP [12]. As pointed out previously, the ESR properties of the free radicals suggest thermal mixing as the main mechanism for ^{13}C DNP. In the thermal mixing model the key to achieving high nuclear polarization is to lower the spin temperature of the electron dipolar system in thermal contact with the nuclear Zeeman system. The narrow ESR *D* of free radicals BDPA and trityl OX063 are beneficial for ^{13}C DNP because it translates to a lower specific heat capacity of the electron spin system [12]. The electron dipolar system can be dynamically cooled by microwave irradiation to a lower spin temperature, the same spin temperature acquired by the nuclear Zeeman system, resulting in higher nuclear polarization. In other words, the narrow ESR *D* of trityl OX063 and BDPA are better matched with the Zeeman energy of low-γ nuclear spins like ^{13}C, resulting in an efficient transfer of polarization from the electrons. Meanwhile, the large ESR *D* of the free radicals galvinoxyl, DPPH and 4-oxo-TEMPO only yielded relatively modest ^{13}C polarization levels. It is likely that these large ESR *D* free radicals are better suited for DNP of high-γ nuclear spins whose nuclear Zeeman energies match the ESR linewidths. For instance, nitroxide-based TEMPO has been shown to polarize ^{1}H spins better than ^{13}C spins via DNP at cryogenic conditions [14, 15].

Preliminary dissolution DNP results—Preliminary results on the ^{13}C dissolution of hyperpolarized trityl-doped [1-^{13}C]pyruvic acid sample from our 4.6 T polarizer into a 600-MHz high resolution Varian Inova NMR spectrometer (Agilent Technologies, Santa Clara, CA) yielded ^{13}C NMR enhancements over 12,000-fold at 14.1 T and 298 K (see Fig. 7a). Figure 7b shows the hyperpolarized decay curve of [1-^{13}C]pyruvate (pH ~7.0) with a calculated liquid-state T_1 close to 40 s under these conditions. The aforementioned NMR signal enhancement corresponds only to about 12 % liquid-state ^{13}C polarization, approximately one-quarter of its enhanced polarization in the solid-state. Two main factors should be taken into account in order to explain this polarization loss. First, the duration of the dissolution process could significantly contribute to polarization decay, mainly due to inherent T_1 relaxation. The high resolution magnet is located around 6 m away from the polarizer and the dissolution transfer time takes about 10–15 s. This is in addition to the time it takes to lift the frozen polarized sample out of the LHe bath and other preparations such as dissolution wand insertion. Second, the magnetic field gradient to which the hyperpolarized liquid is subjected during transfer could also contribute to significant losses in the hyperpolarized signal. In the case of hyperpolarized [1-^{13}C]pyruvate it has been shown in a previous low-field relaxation study that its liquid-state T_1 in the milli-Tesla range is about 50 s and increases to about 60 s as the field gets closer to 1 T [33]. As such, this NMR signal loss may be attributed to other factors. Nevertheless, certain improvements can be made, such as sample preparation, dissolution liquid handling and shortening the transfer time [34]; the use of magnetic rails [35] on the dissolution liquid path can be used to minimize the T_1-related polarization losses in the liquid-state.

Overall solid-state ^{13}C DNP performance—The current DNP polarizer is able to provide substantial ^{13}C solid-state polarization, up to 50 %, a value that is at least on par with or better compared to the results achieved with other homebuilt and commercial DNP polarizers [7, 15–19]. The general design of the polarizer based on an ultra-wide bore superconducting magnet is advantageous because this allows large LHe volume hold of the cryostat and use of a side mount for the microwave cavity. Not having to remove the waveguide prior to dissolution shortens the time from the end of irradiation to when the solution state sample is delivered, increasing the amount of signal that is available for use in the MR experiment. This makes the described system distinct from other homebuilt DNP polarizers [7, 15–19] that employ continuous-flow cryostats drawing LHe from an adjacent LHe dewar.

Conclusion

In this work we constructed an efficient DNP system based on a 150-mm ultra wide-bore superconducting magnet at 4.6 T. A custom-designed 9-L liquid Helium cryostat with a 0.75 L/h consumption rate can be cooled to 1.15 K. The 129-GHz microwave source has a maximum power output of 120 mW and has a wide sweeping range of 1 GHz, which can encompass the full width DNP spectrum of large ESR linewidth free radicals such as 4-oxo-TEMPO. Due to the relatively large LHe capacity of the cryostat the system can support up to 10 h of continuous DNP operation without the need for LHe refill. The large sample space in the cryostat allows use of large volume cups and side mounting of the waveguide bend to

the cavity. ^{13}C polarization levels up to 54 % were achieved in the solid-state for ^{13}C-enriched compounds after DNP. Experimental results have shown that the polarization level achieved is dependent upon a variety of factors, particularly the type of free radical polarizing agents used. Current trends suggest that the narrow ESR linewidth free radicals trityl OX063 and BDPA yielded generally higher ^{13}C polarization levels than the broad linewidth free radicals galvinoxyl, DPPH and 4-oxo-TEMPO. Sample preparation optimization via addition of trace amounts of gadolinium and other lanthanides in the sample [27, 29, 36, 37] or deuteration of the glassing matrix [13, 14]. On the instrumentation side, lowering the operating temperature and increasing the magnetic field of the polarizer [10, 11] may be explored in the future to further amplify the DNP-enhanced nuclear polarization. Our work provides an alternative design of a low-cost DNP system with a relatively large LHe storage capacity that may be suitable for preclinical biomedical MR research.

Acknowledgments

The authors would like to thank Kar Fedosh (Virginia Diodes Inc.) and Tim Reynolds (Kadel Engineering) for helpful technical discussions. This work was supported by the National Institutes of Health (NIH) grant numbers R21EB016197, R21EB009147, R37HL034557, and P41EB015908, the UT Southwestern High Risk/High Impact Grant Award and the Cancer Prevention and Research Institute of Texas grant CPRIT RP-101243.

References

1. Slichter, CP. Principles of magnetic resonance. Springer; New York: 1989.
2. Overhauser AW. Polarization of nuclei in metals. Phys Rev. 1953; 92:411–415.
3. Carver TR, Slichter CP. Experimental verification of the overhauser nuclear polarization effect. Phys Rev. 1956; 102:975–981.
4. Abragam A, Goldman M. Principles of dynamic nuclear polarization. Rep Prog Phys. 1978; 41:395–467.
5. Crabb DG, Meyer W. Solid polarized targets for nuclear and particle physics experiments. Annu Rev Nucl Part Sci. 1997; 47:67–109.
6. Ni QZ, Daviso E, Can TV, Markhasin E, Jawla SK, Swager TM, Temkin RJ, Herzfeld J, Griffin RG. High frequency dynamic nuclear polarization. Acc Chem Res. 2013; 46:1933–1941. [PubMed: 23597038]
7. Ardenkjær-Larsen JH, Fridlund B, Gram A, Hansson G, Hansson L, Lerche MH, Servin R, Thaning M, Golman K. Increase in signal-to-noise ratio of >10,000 times in liquid-state NMR. Proc Natl Acad Sci USA. 2003; 100:10158–10163. [PubMed: 12930897]
8. Gallagher FA, Kettunen MI, Brindle KM. Biomedical applications of hyperpolarized ^{13}C magnetic resonance imaging. Prog Nucl Magn Reson Spectrosc. 2009; 55:285–295.
9. Kurhanewicz J, Vigneron DB, Brindle K, Chekmenev EY, Comment A, Cunningham CH, DeBerardinis RJ, Green GG, Leach MO, Rajan SS, Rizi RR, Ross BD, Warren WS, Malloy CR. Analysis of cancer metabolism by imaging hyperpolarized nuclei: prospects for translation to clinical research. Neoplasia. 2011; 13:81–97. [PubMed: 21403835]
10. Meyer W, Heckmann J, Hess C, Radtke E, Reicherz G, Triebwasser L, Wang L. Dynamic polarization of ^{13}C nuclei in solid ^{13}C labeled pyruvic acid. Nucl Instrum Methods Phys Res, Sect A. 2011; 631:1–5.
11. Johannesson H, Macholl S, Ardenkjaer-Larsen JH. Dynamic nuclear polarization of [1-^{13}C]pyruvic acid at 4.6 tesla. J Magn Reson. 2009; 197:167–175. [PubMed: 19162518]
12. Heckmann J, Meyer W, Radtke E, Reicherz G, Goertz S. Electron spin resonance and its implication on the maximum nuclear polarization of deuterated solid target materials. Phys Rev B. 2006; 74:134418.

13. Lumata L, Merritt ME, Kovacs Z. Influence of deuteration in the glassing matrix on ^{13}C dynamic nuclear polarization. Phys Chem Chem Phys. 2013; 15:7032–7035. [PubMed: 23552448]
14. Kurdzesau F, van den Brandt B, Comment A, Hautle P, Jannin S, van der Klink JJ, Konter JA. Dynamic nuclear polarization of small-labeled molecules in frozen water–alcohol solutions. J Phys D Appl Phys. 2008; 141:155506.
15. Comment A, van der Brandt B, Uffman K, Kurdzesau F, Jannin S, Konter JA, Hautle P, Wenkebach WT, Gruetter R, van der Klink JJ. Design and performance of a DNP prepolarizer coupled to a rodent MRI scanner. Concept Magn Reson Part B. 2007; 31:255–269.
16. Jannin S, Comment A, Kurdzesau F, Konter JA, Hautle P, van der Brandt B, van der Klink JJ. A 140 GHz prepolarizer for dissolution dynamic nuclear polarization. J Chem Phys. 2008; 128:241102. [PubMed: 18601309]
17. Batel M, Krajewski M, Weiss K, With O, Dapp A, Hunkeler A, Gimersky M, Pruessmann KP, Boesiger P, Meier BH, Kozerke S, Ernst M. A multisample 94 GHz dissolution dynamic-nuclear-polarization system. J Magn Reson. 2012; 214:166–174. [PubMed: 22142831]
18. Crémillieux Y, Goutailler F, Montcel B, Grand D, Vermeulen G, Wolf PE. A super-wide bore DNP system for multiple sample preparation: cryogenic performance and polarization at low temperature. Appl Magn Reson. 2012; 43:167–180.
19. Ardenkjaer-Larsen JH, Leach AM, Clarke N, Urbahn J, Anderson D, Skloss TW. Dynamic nuclear polarization polarizer for sterile use intent. NMR Biomed. 2011; 24:927–932. [PubMed: 21416540]
20. Lumata L, Ratnakar SJ, Jindal A, Merritt M, Malloy C, Sherry AD, Kovacs Z. BDPA: an efficient polarizing agent for fast dissolution dynamic nuclear polarization NMR spectroscopy. Chem Eur J. 2011; 17:10825–10827. [PubMed: 21919088]
21. Lumata LL, Merritt ME, Malloy CR, Sherry AD, van Tol J, Song L, Kovacs Z. Dissolution DNP-NMR spectroscopy using galvinoxyl as a polarizing agent. J Magn Reson. 2013; 227:14–19. [PubMed: 23246650]
22. Lumata L, Merritt M, Khemtong C, Ratnakar SJ, van Tol J, Yu L, Song L, Kovacs Z. The efficiency of DPPH as a polarising agent for DNP-NMR spectroscopy. RSC Adv. 2012; 2:12812–12817. [PubMed: 23205273]
23. Conradi MS. Low-temperature NMR techniques. Concepts Magn Reson. 1993; 5:243–262.
24. Kodibagkar V, Conradi MS. Remote tuning of NMR probe circuits. J Magn Reson. 2000; 144:53–57. [PubMed: 10783273]
25. Thomas Jefferson National Lab. Userweb Helium vapor pressure vs temperature. https://userweb.jlab.org/~ckeith/TOOLS/HeVaporTable.html
26. Jannin S, Bornet A, Melzi R, Bodenhausen G. High field dynamic nuclear polarization at 6.7 T: carbon-13 polarization above 70 % within 20 min. Chem Phys Lett. 2012; 549:99–102.
27. Lumata L, Merritt ME, Malloy CR, Sherry AD, Kovacs Z. Impact of Gd^{3+} on DNP of [1-^{13}C]pyruvate doped with trityl OX063, BDPA, or 4-oxo-TEMPO. J Phys Chem A. 2012; 116:5129–5138. [PubMed: 22571288]
28. Lumata L, Merritt ME, Malloy C, Sherry AD, Kovacs Z. Fast dissolution dynamic nuclear polarization NMR of ^{13}C-enriched ^{89}Y-DOTA complex: experimental and theoretical considerations. Appl Magn Reson. 2012; 43:69–79.
29. Lumata L, Jindal AK, Merritt ME, Malloy CR, Sherry AD, Kovacs Z. DNP by thermal mixing under optimized conditions yields >60,000-fold enhancement of ^{89}Y NMR signal. J Am Chem Soc. 2011; 133:8673–8680. [PubMed: 21539398]
30. Borghini M. Spin-temperature model of nuclear dynamic polarization using free radicals. Phys Rev Lett. 1968; 20:419–421.
31. Jannin S, Comment A, van der Klink JJ. Dynamic nuclear polarization by thermal mixing under partial saturation. Appl Magn Reson. 2012; 43:59–68.
32. Lumata L, Kovacs Z, Malloy C, Sherry AD, Merritt M. The effect of ^{13}C enrichment in the glassing matrix on dynamic nuclear polarization of [1-^{13}C]pyruvate. Phys Med Biol. 2011; 56:N85–N92. [PubMed: 21285486]

33. Chattergoon N, Martínez-Santiesteban F, Handler WB, Ardenkjær-Larsen JH, Scholl TJ. Field dependence of T_1 for hyperpolarized [1-^{13}C]pyruvate. Contrast Media Mol Imaging. 2013; 8:57–62. [PubMed: 23109393]

34. Cheng T, Mishkovsky M, Bastiaansen JAM, Ouari O, Hautle P, Tordo P, van der Brandt B, Comment A. Automated transfer and injection of hyperpolarized molecules with polarization measurement prior to in vivo NMR. NMR Biomed. 2013; 26:1582–1588. [PubMed: 23893539]

35. Bornet A, Melzi R, Linde AJP, Hautle P, van der Brandt B, Jannin S, Bodenhausen G. Boosting dissolution dynamic nuclear polarization by cross polarization. J Phys Chem Lett. 2013; 4:111–114.

36. Gordon JW, Fain SB, Rowland IJ. Effect of lanthanide ions on dynamic nuclear polarization enhancement and liquid-state T_1 relaxation. Magn Reson Med. 2012; 68:1949–1952. [PubMed: 22367680]

37. Waldner LF, Chen A, Mander W, Scholl T, McKenzie C. Optimisation of dynamic nuclear polarisation of [1-^{13}C] pyruvate by addition of gadolinium-based contrast agents. J Magn Reson. 2012; 223:85–89. [PubMed: 22975238]

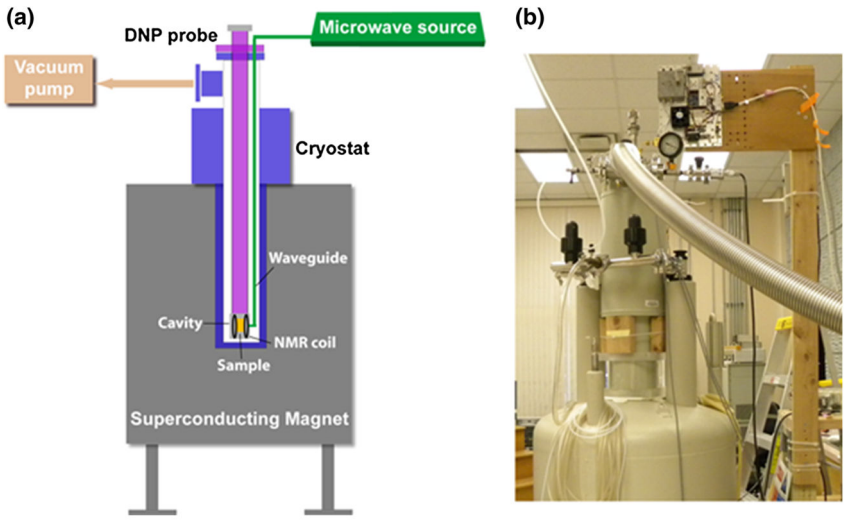

Fig. 1.

a General schematic diagram of the homebuilt DNP machine showing the main components: cryostat, superconducting magnet, DNP probe, microwave source, vacuum pump, and NMR system; **b** photograph of the actual DNP polarizer based on the design shown in **a**

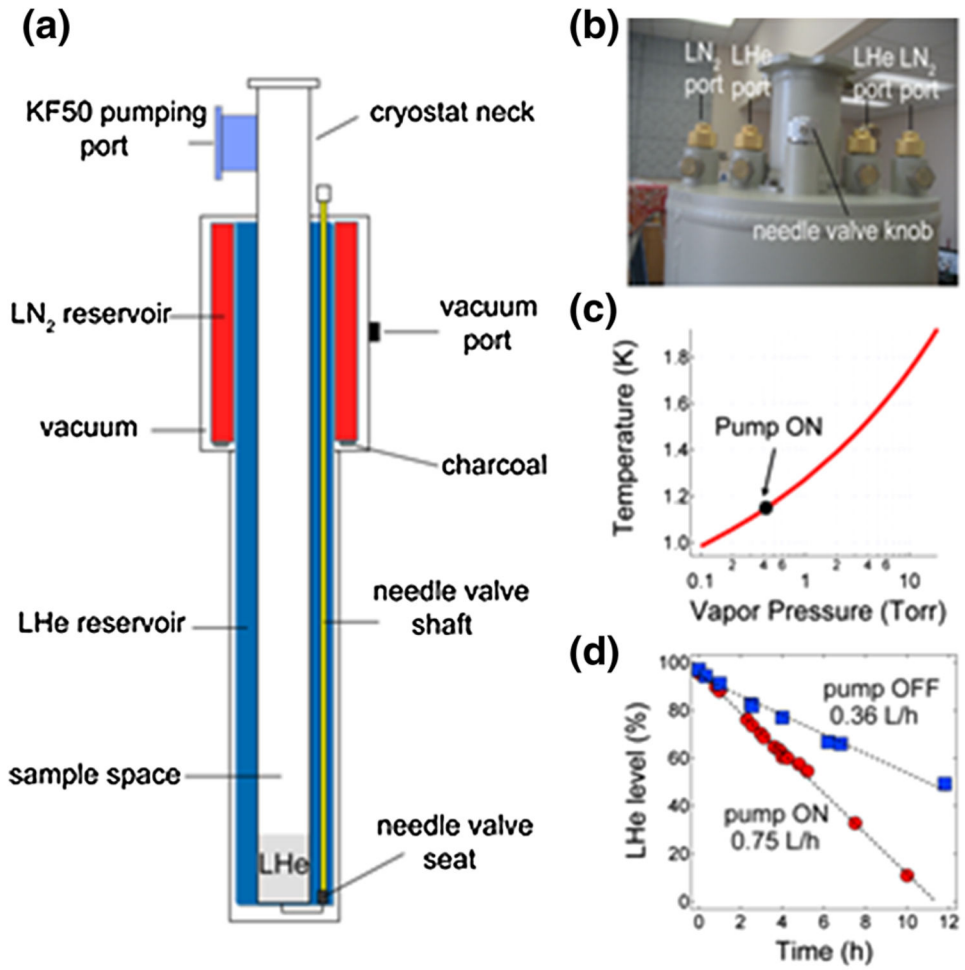

Fig. 2.

a Schematic diagram of the cryostat with the main components: LHe (9 L capacity) and LN_2 (5 L capacity) reservoirs, sample space, needle valve components, pumping ports and other parts; **b** Photograph of the top portion of the cryostat showing the filling ports for the cryogens as well as the needle valve knob; c Plot of the temperature versus the LHe vapor pressure [25]. The *solid circle* indicates the LHe bath temperature (1.15 K) achieved for the sample when the pump is on; **d** Liquid helium boil off rates of the cryostat main reservoir (9 L at 100 % level) with the pump on or off. The *dashed lines* are fits to a linear equation where the calculated boil off rates are 0.75 L/h with the pump on and 0.36 L/h when the pump is off

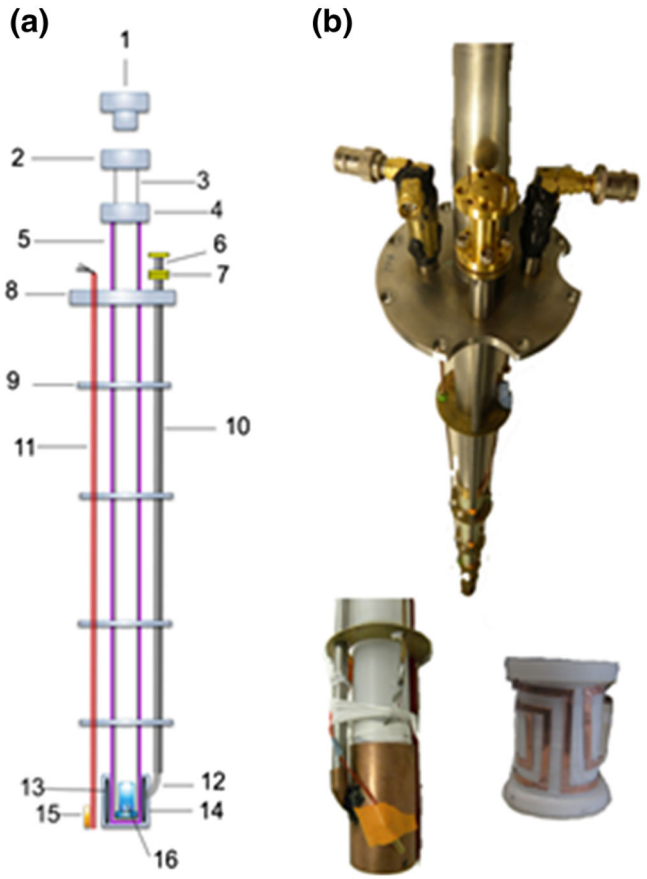

Fig. 3.

DNP probe insert. **a** Schematic diagram of the DNP probe: (*1*) brass plug, (*2* and *4*) coupling pieces, (*3*) inner sliding tube, (*5*) outer support tube, (*6*) rectangular to circular transition waveguide, (*7*) homebuilt waveguide adapter, (*8*) stainless steel plate, (*9*) brass plate heat shields, (*10*) stainless tube waveguide, (*11*) liquid helium level sensor, (*12*) 90° waveguide bend, (*13*) NMR saddle coil, (*14*) microwave cavity, (*15*) temperature sensor and (*16*) sample cup; **b** Photographs of the DNP probe showing the two NMR ports and microwave waveguide (*top*), as well the microwave cavity (*bottom left*) and the rectangular saddle NMR coil inside the cavity (*bottom right*)

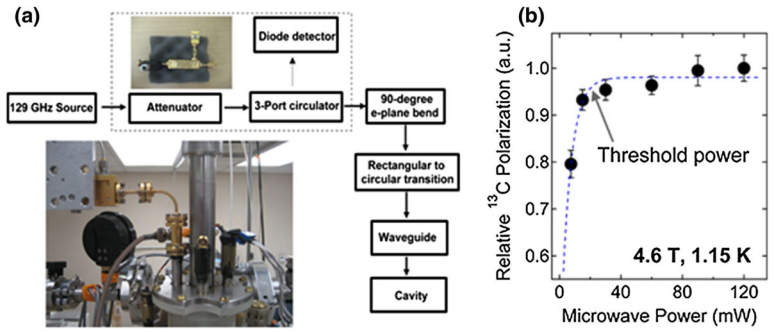

Fig. 4.

a Schematic diagram of the 129-GHz microwave system used for DNP. The components within the *dashed box* (attenuator-3 port circulator-diode detector) can be bypassed during DNP. *Insets* photographs of the top section of the microwave system. **b** Relative ^{13}C polarization level of trityl-doped [1-^{13}C]pyruvic acid sample (see Table 1) as a function of microwave power at 4.6 T and 1.1 K where the threshold microwave power is around 20 mW. Data were plotted by obtaining the maximum ^{13}C NMR intensity after microwave irradiation of the sample at the positive polarization peak. Microwave power was controlled by a variable attenuator and the power was measured with a diode detector. The *dashed curve* is a guide for the eyes

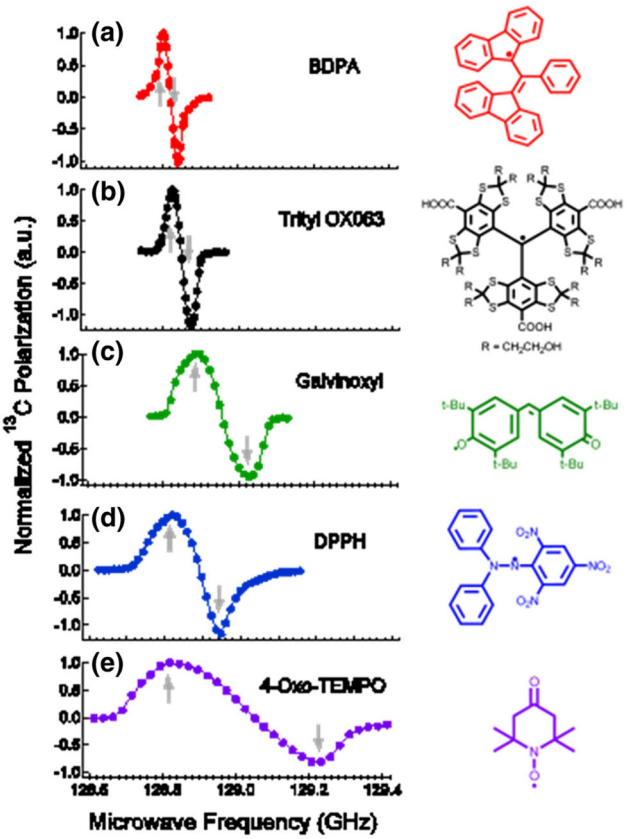

Fig. 5.

^{13}C microwave DNP spectra of ^{13}C-enriched substrates doped with **a** BDPA, **b** trityl OX063, **c** galvinoxyl, **d** DPPH, and **e** 4-oxo-TEMPO (see Table 1 for details of sample composition) taken at 4.6 T and 1.15 K with a 120 mW microwave source. The *up* and *down arrows* correspond to the positive *P*(+) and negative *P*(−) polarization peaks, respectively. The corresponding chemical structures of the free radicals are displayed on the right

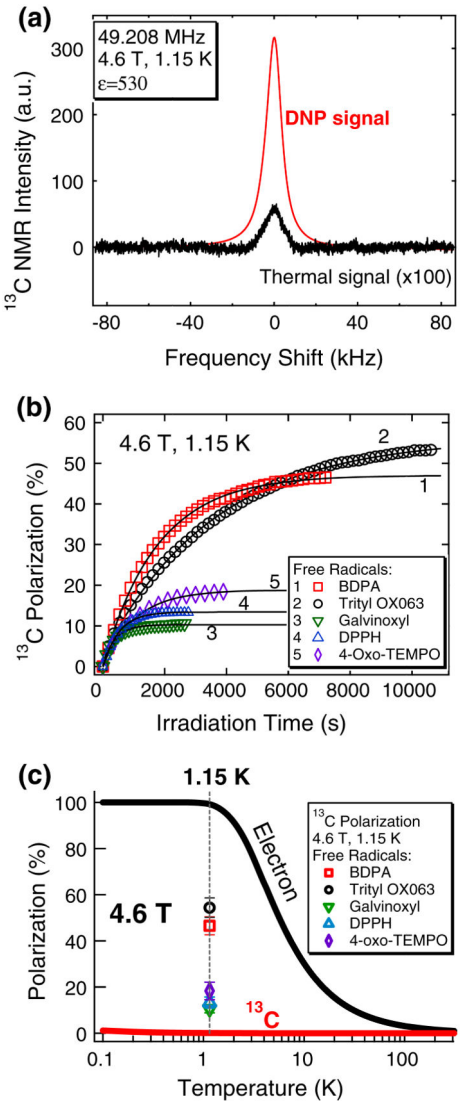

Fig. 6.

a Representative DNP and thermal ^{13}C NMR signals of neat [1-^{13}C]pyruvic acid doped with 15 mM trityl OX063 measured at 4.6 T and 1.15 K. The calculated NMR signal enhancement ε of this particular frozen polarized ^{13}C sample was 530, which corresponds to 54 % ^{13}C polarization under these conditions. **b** ^{13}C polarization buildup curves of ^{13}C samples doped with (*1*) BDPA, (*2*) trityl OX063, (*3*) galvinoxyl, (*4*) DPPH and (*5*) 4-oxo-TEMPO (see Table 1 for sample composition). The ^{13}C samples were irradiated at the positive polarization peak (+) at 4.6 T and 1.15 K with a 120 mW microwave source. The *solid lines* are fits to a single-exponential buildup equation with a buildup time constant τ_{bu}. **c** Calculated temperature dependence of Boltzmann thermal electron and ^{13}C nuclear polarization levels at 4.6 T. Experimental values of DNP-enhanced ^{13}C polarization levels of ^{13}C samples doped with different free radicals using the homebuilt DNP polarizer at 4.6 T and 1.15 K are displayed as symbols (see Table 1 for details of sample composition)

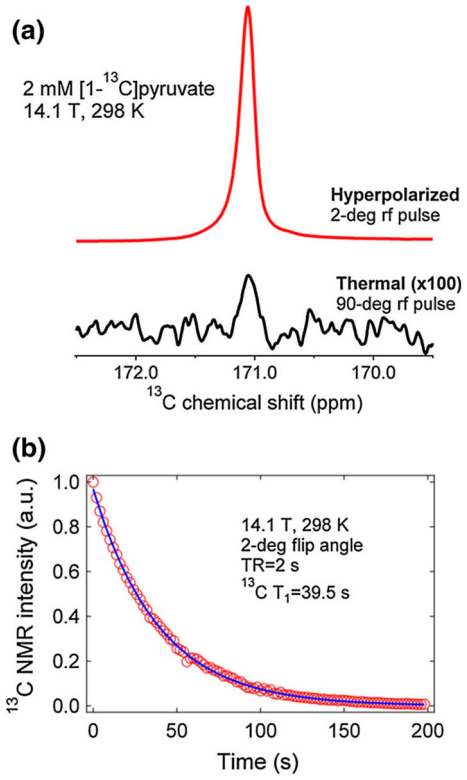

Fig. 7.

a Representative ^{13}C hyperpolarized (2° flip angle) and thermal (90° flip angle) NMR spectra of 2 mM [1-^{13}C]pyruvic acid taken at 14.1 T and 298 K after dissolution of frozen polarized trityl-doped sample at 4.6 T and 1.15 K. The calculated liquid-state NMR signal enhancement is about 12,000-fold. **b** Decay of the liquid-state NMR signal emanating from hyperpolarized [1-^{13}C]pyruvic acid at 14.1 T and 298 K. The decay curve was monitored by applying a 2° rf pulse every 2 s. These data were fitted with a decay equation accounting for the effects of rf pulse and T_1 relaxation [29]

Table 1

Sample composition (free radical polarizing agents, radical concentration *c*, ^{13}C-labelled substrates and glassing matrices) and ^{13}C DNP parameters (positive *P*(+) and negative *P*(−) polarization peaks, buildup time constant τ_{bu}, and DNP-enhanced ^{13}C polarization *P*)

Free radical	*c* (mM)	^{13}C substrate and glassing matrix	*P*(+)/*P*(−) (GHz)	τ_{bu} (s)	^{13}C P_{dnp} (%)
BDPA	20	1:1 (v/v) [1-^{13}C]pyruvic acid:sulfolane	128.80/128.84	1,770 ± 150	46.5 ± 3.9
Trityl OX063	15	Neat [1-^{13}C]pyruvic acid	128.82/128.88	3,310 ± 120	54.4 ± 4.2
Galvinoxyl	40	1:1 (v/v) [1-^{13}C]ethyl acetate:DMSO	128.90/129.03	388 ± 20	10.5 ± 1.7
DPPH	20	1:1 (v/v) [1-^{13}C]ethyl acetate:sulfolane	128.82/128.95	531 ± 46	13.3 ± 2.4
4-Oxo-TEMPO	40	1.4 M [1-^{13}C]sodium pyruvate in 1:1 (v/v) glycerol:water	128.82/129.23	1058 ± 72	18.3 ± 3.8

The ^{13}C samples (*N* = 3 for each free radical) were polarized by microwave irradiation at P(+) with a 120 mW microwave source. The corresponding ^{13}C polarization *P* and τ_{bu} values were measured at 4.6 T and 1.15 K. The error values for *P* and τ_{bu} are standard deviations of *N* = 3 trials